ADVANCED FUNCTIONAL MATERIALS
www.afm-journal.de

Control of Ambipolar and Unipolar Transport in Organic Transistors by Selective Inkjet-Printed Chemical Doping for High Performance Complementary Circuits

Dongyoon Khim, Kang-Jun Baeg, Mario Caironi, Chuan Liu, Yong Xu, Dong-Yu Kim,* and Yong-Young Noh**

The selective tuning of the operational mode from ambipolar to unipolar transport in organic field-effect transistors (OFETs) by printing molecular dopants is reported. The field-effect mobility (μ_{FET}) and onset voltage (V_{on}) of both for electrons and holes in initially ambipolar methanofullerene [6,6]-phenyl-C61-butyric acid methyl ester (PCBM) OFETs are precisely modulated by incorporating a small amount of cesium fluoride (CsF) n-type dopant or tetrafluoro-tetracyanoquinodimethane (F4-TCNQ) p-type dopant for n-channel or p-channel OFETs either by blending or inkjet printing of the dopant on the pre-deposited semiconductor. Excess carriers introduced by the chemical doping compensate traps by shifting the Fermi level (E_F) toward respective transport energy levels and therefore increase the number of mobile charges electrostatically accumulated in channel at the same gate bias voltage. In particular, n-doped OFETs with CsF show gate-voltage independent Ohmic injection. Interestingly, n- or p-doped OFETs show a lower sensitivity to gate-bias stress and an improved ambient stability with respect to pristine devices. Finally, complementary inverters composed of n- and p-type PCBM OFETs are demonstrated by selective doping of the pre-deposited semiconductor via inkjet printing of the dopants.

1. Introduction

Ambipolar organic field-effect transistors (OFETs), devices which can operate both in the electron and hole accumulation regime, have seen tremendous progress in recent years, both favored by an evolutionary design of conjugated molecules and by an improved understanding of the mechanism of charge transport in molecular solids.[1–4] A wide variety of semiconducting materials from conventional silicon to recently studied nanoribbon graphene, reduced graphene oxide, single-walled carbon nanotubes, quantum dots and organic semiconductors exhibit the ambipolar characteristics.[5–12] Among them, the interesting features of π-conjugated molecules is that ambipolar properties can be tuned by controlling the chemical structure of the organic semiconductors, by engineering charge injection properties and by carefully selecting the gate dielectric layers.[3,4,13–19] A representative application which exploits ambipolar properties is the light-emitting transistor, which can emit light upon the formation and the successive radiative decay of an exciton in the channel populated by both holes and electrons.[5,20,21] Furthermore, solution processability enables to realize organic complementary integrated circuits thanks to simple coating or printing of a single layer of an ambipolar conjugated molecule, without the need for fine patterning through conventional photopatterning processes.[22–27]

To develop high performance complementary circuits based on ambipolar materials, several requirements are to be met: 1) high hole and electron mobility, 2) efficient hole and electron injection from the electrodes, and 3) high on/off ratio through the unipolarization of the device.[23] Even though conjugated molecules can commonly transport both electron and hole, it is not trivial to achieve comparable mobility values in the same material. This is because hole and electron mobilities in OFETs are determined by many concomitant factors,

D. Khim, C. Liu, Prof. Y. Xu, Prof. Y.-Y. Noh
Department of Energy and Materials Engineering
Dongguk University
26 Pil-dong, 3-ga, Jung-gu
Seoul 100–715, Republic of Korea
E-mail: xu.yong@dongguk.edu; yynoh@dongguk.edu

D. Khim, Prof. D.-Y. Kim
Heeger Center for Advanced Materials
School of Materials Science and Engineering
Gwangju Institute of Science and Technology (GIST)
1 Cheomdan-gwagiro, Buk-gu, Gwangju 500–712, Republic of Korea
E-mail: kimdy@gist.ac.kr

K.-J. Baeg
Nano Carbon Materials Research Group
Korea Electrotechnology Research Institute (KERI)
12, Bulmosan-ro 10beon-gil, Seongsan-gu
Changwon, Gyeongsangnam-do
642–120, Republic of Korea

M. Caironi
Center for Nano Science and Technology @PoliMi
Istituto Italiano di Tecnologia
Via Pascoli 70/3, 20133, Milano, Italy

DOI: 10.1002/adfm.201400850

both intrinsic (e.g., molecular structure, morphology, etc.) and extrinsic (e.g., trapping of carriers at interfaces, contaminants, etc.) and because we lack general transport models capable of predicting OFET properties. While general molecular design approaches have been developed to obtain both high electron and hole mobility, such as alternating donor and acceptor moieties in the case of polymers,[23,28] most of the development in order to obtain a well-balanced hole and electron mobility in a device is empirical and we do not have a theoretical framework capable of rationalizing it. Secondly, if not enough care is paid, it is very common to observe inefficient injection of at least one of the two carrier species mainly due to a large injection barrier between a single metal work-function and the frontier energetic levels of organic semiconductors. In addition, with the perspective of fabricating complementary circuits, V-shaped transfer characteristics of typical ambipolar OFETs are very unsuitable[1] as they lead to abnormal Z-shaped characteristics of inverters with a large static power consumption and limited noise immunity.[22,23] To solve these problems, the characteristics of devices based on ambipolar materials must be optimized for efficient injection and transport of only one of the two carriers, selectively. There have been several approaches to selectively control the polarity of ambipolar OFETs, such as the introduction of trap-free gate dielectrics, the blending of different dielectrics, the insertion of specific charge injection interlayers, and the modification of the work function of contact electrodes by self-assembled monolayers (SAMs).[4,13–19] However, successful approaches to selectively control transistor operation modes through chemical doping are rare.[29]

Herein, we report on a simple yet effective method to tune the balance between hole and electron mobility in OFETs based on an ambipolar molecule by chemical doping. Chemical doping represents a very effective method to control injection and transport properties in electronic devices and, although of limited use so far in solution-processed organic devices, many reports are present in the literature on the fundamental studies and application of this approach.[29–40] The effective field-effect mobility (μ_{FET}) and onset voltage (V_{on}) of both electrons and holes in initially ambipolar methanofullerene [6,6]-phenyl-C61-butyric acid methyl ester (PCBM) OFETs are precisely modulated by blending or selective inkjet printing of a small amount of cesium fluoride (CsF) as n-type dopant and tetrafluoro-tetracyanoquinodimethane (F4-TCNQ) as p-type dopant for n-channel and p-channel OFETs, respectively. This neat effect is mainly attributed to the Fermi level (E_F) shift towards the transport energy levels in PCBM upon chemical doping, resulting in a conversion from ambipolar to unipolar OFETs. Doping increases the concentration of excess carriers of one kind in the channel, filling deep trap states in the corresponding density of states (DOS), while reducing the concentration of the other carrier species, thus depopulating highly localized states in this case; simultaneously, doping is effective in decreasing the charge injection barrier for the charge carriers. Interestingly, p- or n-doped unipolar OFETs showed greater stability than ambipolar devices under the same gate-bias stress and ambient conditions, mostly due to the filling of deep trap states consequent to the shift of E_F closer to the corresponding transport energy levels. Finally, we demonstrate remarkably improved complementary-like organic inverters based on n-doped and p-doped PCBM OFETs as n-channel and p-channel transistors by selective inkjet printing on top of the pre-deposited semiconductor of CsF and F4-TCNQ dopant, respectively. The PCBM only complementary inverters exhibit a high voltage gain of ≈14 and excellent noise margins, as high as 67% of $^1/_2\ V_{dd}$.

2. Results and Discussion

F4-TCNQ and CsF were chosen as p- and n-dopant because they are well known as efficient dopants in the field of organic opto-electronics and can be easily dissolved in common organic solvents such as chlorobenzene(CB) and 2-ethoxyethanol, facilitating blends with π-conjugated organic semiconductors.[31] In order to obtain n-type doping to organic semiconductors the dopants have to donate electrons to the lowest unoccupied molecular orbital (LUMO) states, while p-type dopants extract electrons from the highest occupied molecular orbital (HOMO) state, therefore generating holes.[30,31] In our system, since the E_F of CsF (1.9–2.0 eV) is well above the LUMO levels of typical organic semiconductors, electron transfer from cesium compound into LUMO of PCBM (≈3.7 eV) is energetically favorable with likely n-type doping. In contrast to other reactive metal dopant, incorporation of cesium compound into organic layer can lead to the n-doping without strong chemical reaction and formation of gap states, implying cesium compound can serves as a stable n-type dopant.[41] F4-TCNQ has deep LUMO (5.2–5.4 eV), which is favorable to extract electron of semiconductors in the vicinity of dopant such that holes are generated in PCBM like p-doping.[30,31] From the ultraviolet photoelectron spectroscopy (UPS), **Figure 1**a,b shows a gradual shift in E_F from the value of pristine PCBM upon increasing the concentration of either F4-TCNQ (p-doped) or CsF (n-doped) from 0.1 to 1.0 wt%. It reveals that E_F, depending on the doping, can be markedly shifted towards the HOMO for p-doping and towards the LUMO for n-doping. Beyond the critical doping concentration of 1.0 wt%, the E_F of both n- and p-doped PCBM was pinned, presumably due to a high density of tailing states within the transport gap or full compensation of the donor (acceptor) states by dopants, which leads to saturation of E_F shift at high doping ratio.[42] As summarized in **Table 1**, the resulting E_F decreases from −4.13 to −4.63 eV (ΔE_F = 0.5 eV) and increases from −4.12 to −3.80 eV (ΔE_F = 0.32 eV) at a doping concentration of 1.0 wt% by F4-TCNQ and CsF in PCBM, respectively. Obviously, such shifts in E_F can substantially change the concentration of thermally promoted excess carriers in the active semiconductor layer. Interestingly, E_F of undoped PCBM is located above the intrinsic Fermi level (E_{Fi}), which means that pristine PCBM could be regarded as native n-type semiconductor.

The effect of dopant on the morphology of PCBM thin film is investigated by atomic force microscopy (AFM) (See Figure S1 and S2 in Supporting Information). The morphology of F4-TCNQ-doped PCBM thin film is very similar with that of pristine PCBM, exhibiting very smooth and no explicit change by incorporation of dopant, whereas CsF-doped PCBM film shows significant different morphology with needle-like aggregation of dopant. It may be due to relatively poor solubility of

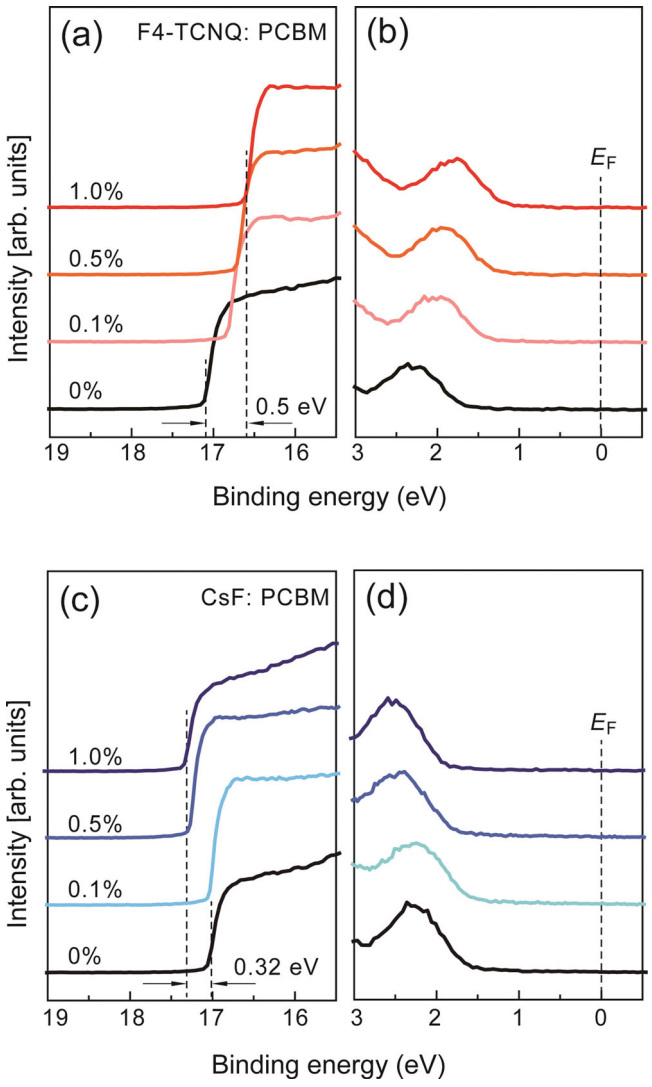

Figure 1. UPS spectra showing the evolution of the PCBM HOMO with increasing doping level a) F4-TCNQ as p-dopant, b) CsF as n-dopant.

CsF in PCBM solution based on CB, which could lead to extraction or aggregation of CsF during spin-coating.

To investigate the doping effect on the electrons and holes transport, we fabricated top-gate/bottom-contact (TG/BC) OFET devices by using pristine and doped PCBM solutions. A detailed description of the fabrication process is given in the Experimental section. Our staggered OFETs have relatively low contact resistance (R_c) due to large physical contact area and reduced current crowding effect.[43] The perfluoropolymer, CYTOP which is a low-*k*, chemically stable, low surface energy and hydrophobic gate dielectric, can be dissolved in perfluorosolvents perfectly orthogonal to under-laid solution-processable organic semiconductors including PCBM.[44] Therefore, it enables the investigation of the active layer doping effect excluding well-known extrinsic contributions, such as interfacial traps and doping or charge trapping by oxygen and/or moisture in air. As it can be seen in **Figure 2**, the pristine (undoped) PCBM OFETs show V-shape transfer characteristics of typical ambipolar transistors. Notably, we used gold (Au) bottom-contact electrodes, whose work function may reduce to ≈–4.5 eV compared to that of atomically clean Au bulk (≈–5.1eV) because of pushed-back electron tails by adsorbed hydrocarbon molecules onto the metal electrode surface.[44] Consequently, the charge injection barriers to electrons and holes are approximately 0.8 eV and 1.2 eV, respectively. Here we assume the Schottky-Mott limit and the injection barrier is simply the difference between LUMO (or HOMO) and the metal work-function for simplicity. Despite the large injection barrier height, we obtained relatively high effective field-effect mobilities of 0.067 (±0.0092) $cm^2\ V^{-1}\ s^{-1}$ and 0.030 (±0.0026) $cm^2\ V^{-1}\ s^{-1}$ for n-channel ($\mu_{FET,e}$) and p-channel ($\mu_{FET,h}$) regime, respectively, which are much higher than those of previously reported ambipolar PCBM OFETs with bottom-gate/bottom-contact coplanar device structure and SiO_2 gate dielectric.[46,47] This improvement mainly results from the simultaneous enhancement of charge injection from bottom-contact electrodes in a staggered architecture and charge transport at the semiconductor–dielectric interface.

A small amount of dopants in the PCBM active layer leads to noticeable change in the OFET device performance. Figure 2a,b shows the evolution of the p-channel (at the drain voltage $V_d = -60$ V) and *n*-channel (at $V_d = +60$ V) transfer characteristics of n-doped PCBM OFETs by CsF, while Figure 2c,d shows the same evolution of the p-channel (at $V_d = -60$ V) and n-channel (at $V_d = +60$ V) transfer characteristics of p-doped PCBM OFETs by F4-TCNQ, respectively. In Figure 2a, an initially ambipolar device with almost balanced currents, is gradually turned into a unipolar, n-type OFET with increasing CsF doping concentration from 0.1 wt% to 1.0 wt%. CsF doping shifts the transfer curves in the direction of more negative gate bias, thus increasing n-channel saturation current while reducing p-channel current. Note that at higher doping levels of above 2.0 wt%, only OFF-current (I_{off}) was increased up to 1.95×10^{-8}, ~38 times higher than in the case of the 1.0 wt% doped OFET device (5.06×10^{-10} A), but without significant difference in ON-current (See Figure S3 in Supporting Information).[39] For p-doping by F4-TCNQ, on the other hand, hole current is only slightly increased, whilst the electron transport is severely limited under the both p- and n-channel operation regions (see Figure 2c). This indicates that the polarity and density of excess charge carriers can be modulated by appropriate p- or n-doping at specific doping levels, leading to a substantial unipolarization of devices and to an overall enhancement of device performance, in terms of increase in saturation current and decrease in threshold voltage (V_{th}). The measured μ_{FET}, V_{th}, and V_{on} of all devices are summarized in **Table 2**.

Figure 3a,b exhibits μ_{FET} and V_{on} trends upon doping PCBM OFETs with various doping ratio. For 1.0 wt% CsF-doped OFETs, the $\mu_{FET,e}$ and $\mu_{FET,h}$ were remarkably changed from 0.067 $cm^2\ V^{-1}\ s^{-1}$ and 0.030 $cm^2\ V^{-1}\ s^{-1}$ to 0.13 $cm^2\ V^{-1}\ s^{-1}$ and 5.9×10^{-5} $cm^2\ V^{-1}\ s^{-1}$, respectively, resulting in an almost negligible holes transport. On the contrary, F4-TCNQ-doped OFETs (1.0 wt%) exhibited only a slight modification in $\mu_{FET,h}$, increased up to 0.045 $cm^2\ V^{-1}\ s^{-1}$, while featuring a drastic decrease in $\mu_{FET,e}$, reducing to 7.9×10^{-4} $cm^2\ V^{-1}\ s^{-1}$. As shown in Figure 3a, PCBM OFETs can be tuned to exhibit three different operation regimes: i) equivalent ambipolar transport with pristine PCBM, ii) n-channel predominant operation with n-doped PCBM, and iii) p-channel predominant operation with

Table 1. Summary of Fermi level and hole and electron concentrations of the doped PCBM films, corresponding depletion width of interface between Au and doped PCBM.

Dopant	Dopant concentration [wt%]	Fermi level [eV]	Hole or electron concentration[a] [cm^{-3}]	Depletion width (majority carrier)[b]
F4-TCNQ (*p*-doping)	Intrinsic	4.13	3.73×10^{-6}	>1 μm
	0.1	4.39	8.90×10^{-2}	>1 μm
	0.5	4.52	1.37×10^{1}	>1 μm
	1.0	4.63	9.74×10^{2}	>1 μm
CsF (*n*-doping)	Intrinsic	4.12	8.51×10^{13}	>1 μm
	0.1	4.13	5.78×10^{13}	>1 μm
	0.5	3.91	2.92×10^{17}	29.54 nm
	1.0	3.80	2.07×10^{19}	3.86 nm

[a]F4-TCNQ doped film: hole, CsF doped film: electron. The very low hole concentrations after p-doping is for the intrinsic condition at thermal equilibrium. The hole concentration can be much increased upon applying negative gate voltage, due to the injection of excess holes from contacts, which is why we can still observe good p-type transistor characteristics; [b]The large depletion widths are simply denoted as >1 μm because tunneling cannot happen at such a large thickness over 1 μm.

p-doped PCBM. Corresponding V_{on} shifts of the same devices are displayed in Figure 3b, evidencing the effective control on V_{on} by appropriate doping level: from −18.6 (±0.91) V to −68.9 (±6.48) V and from −3.5 (±0.4) V to 56.6 (±5.8) V in p-channel and n-channel operation regimes, respectively.

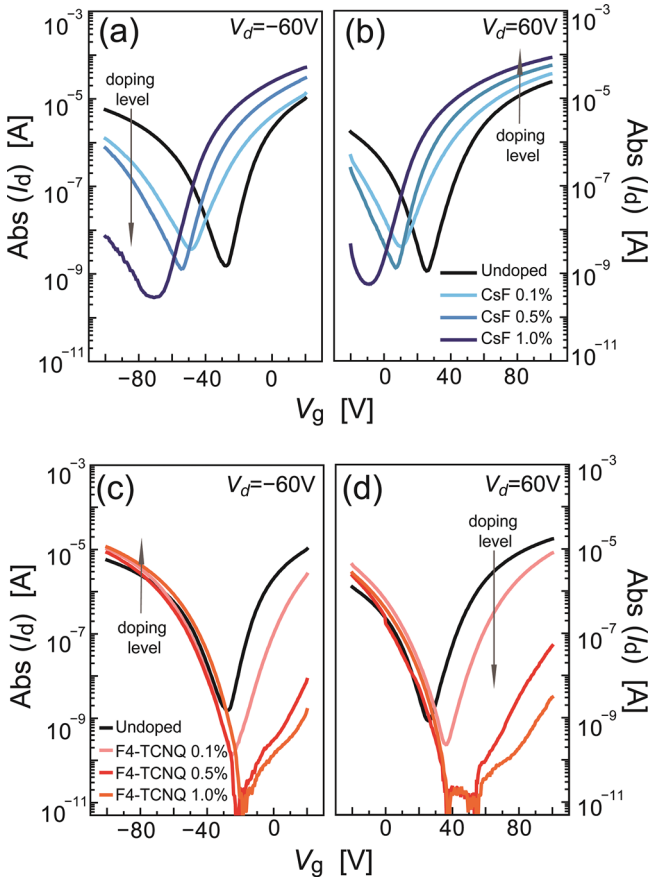

Figure 2. Transfer characteristics of a) CsF-doped PCBM OFETs (p-channel) and b) (n-channel). c) F4-TCNQ-doped OFETs (p-channel) and d) (n-channel) at varying doping concentration.

The V_{on} is defined as the voltage at which the mobile charges begin to accumulate in the channel. For ambipolar FETs, especially, it could be interpreted as the voltage at which the transport carrier types change from electrons (holes) to holes (electrons) under the negative (positive) gate bias conditions.[1] Because p- or n-doping shifts the E_F towards their corresponding transport energy levels, the increased density of filled localized states leads to improvement of the device characteristics in the corresponding operation mode. In fact, organic semiconductors with low degree of long-range order are typically affected by energetic disorder, also determined by chemical defects and impurities. This leads to an electronic structure characterized by a DOS of localized states centered around HOMO and LUMO levels, where transport is typically described by hopping.[48] If we refer to the electrons case, deep intra-gap levels in the DOS can strongly reduce carriers mobility, since at room temperature the hopping rate to higher lying levels, leading to improved conductivity, is very limited. Therefore, by chemically increasing the excess electrons concentration and consequently moving the E_F higher in the DOS, deep levels are populated so that the additional carriers introduced by electrostatic coupling in the transistor tend to occupy energy levels closer to transport levels, resulting in an improved mobility. Indeed, it has been extensively reported that charge carrier mobility in OFETs increase with the charge concentration in active layer that often manifests as a gate-voltage enhanced mobility.[49,50]

Another crucial aspect leading to improved device performances thanks to the doping procedure here adopted is the simultaneous enhancement of the charge injection properties. **Figures 4**a–d show the p- and n-channel output characteristics of pristine or doped PCBM OFETs. The super-linear curves at small V_d values in pristine devices are mostly attributed to large charge injection barriers from bottom-contact Au electrodes experienced by both electrons and holes. The resulting large contact resistances can be strongly reduced upon p-doping (for holes) and n-doping (for electrons) by F4-TCNQ and CsF, respectively. This is first evidenced in an increased drain current (I_d) and better linearity in output plots at small V_d, especially in the electrons case for CsF doping. We evaluated the contact resistance (R_c) by using a modified version of the

Table 2. TG/BC OFET parameters for PCBM with various doping ratio. The electrical parameters were calculated at the saturation region ($V_d = \pm 60$ V) using gradual approximation equations [W/L = 1.0 mm/20 μm].

OSC	Dopant Concentration	n-channel			p-channel		
		$\mu_{FET,e}$ [$cm^2V^{-1}s^{-1}$]	$V_{th,e}$ [V]	$V_{on,e}$ [V]	$\mu_{FET,h}$ [$cm^2V^{-1}s^{-1}$]	$V_{th,h}$ [V]	$V_{on,h}$ [V]
PCBM	Intrinsic	0.067 (±0.00917)	45.93 (±7.43)	26.7 (±3.1)	0.030 (±0.0026)	−46.4 (±6.92)	−28.3 (±6.2)
	CsF (0.1 wt%)	0.090 (±0.00577)	37.6 (±1.38)	9.5 (±0.5)	0.012 (±0.00059)	−54.9 (±0.35)	−47.4 (±0.5)
	CsF (0.5 wt%)	0.10 (±0.0075)	24.3 (±1.88)	8.3 (±1.2)	0.011 (±0.0045)	−72.2 (±1.60)	−54.3 (±2.3)
	CsF (1.0 wt%)	0.13 (±0.0057)	15.4 (±0.21)	−3.5 (±0.4)	5.9×10^{-5} ($\pm 4.6 \times 10^{-5}$)	−79.4 (±4.67)	−68.9 (±6.48)
	F4-TCNQ (0.1 wt%)	0.070 (±0.018)	65.6 (±1.4)	35.5 (±1.6)	0.044 (±0.0015)	−50.0 (±1.45)	−25.2 (±2.2)
	F4-TCNQ (0.5 wt%)	0.0019 (±0.0013)	81.2 (±7.3)	53.4 (±6.1)	0.045 (±0.0025)	−54.2 (±1.65)	−21.5 (±2.4)
	F4-TCNQ (1.0 wt%)	7.9×10^{-5} ($\pm 1.0 \times 10^{-5}$)	80.1 (±8.8)	56.6 (±5.8)	0.045 (±0.0038)	−48.6 (±1.28)	−18.6 (±0.91)

transfer-length method (TLM). In the modified-TLM (M-TLM), the error that is caused by parameters dispersion related to the channel resistance is minimized by changing the linear regression from channel-resistance based to contact-resistance based, leading to a more reliable extraction (see **Figure 5**).[51] R_c is estimated from the slope of $1/L$ with L being the channel length, as shown by the following equation:

$$\frac{R_{total} \times W}{L} = \frac{1}{\mu C_i (V_G - V_{th})} + (R_c \times W)\frac{1}{L} \quad (1)$$

where R_{total} is the total resistance, W the channel width, C_i the unit area capacitance of the gate dielectric, and V_G the gate voltage, respectively. One can first see from Figure 5 that the intrinsic PCBM OFETs suffer from very high R_c in n-channel regime, and even higher in the case of p-channel, a major limitation of the overall device characteristics. Upon doping, R_c for p-type conduction is considerably decreased by more than one order of magnitude (from 1.39 MΩ cm to 0.26 MΩ cm at $V_g = -100$ V and $V_d = -10$ V for F4-TCNQ doping), while R_c for n-type conduction becomes almost negligible (from 1.65×10^5 Ω cm to 1.57×10^2 Ω cm at $V_g = 100$ V and $V_d = 10$ V for CsF doping). The R_c value achieved for electrons is remarkably low in the context of OFETs and, interestingly, it results independent of the gate voltage. This R_c is obtained from the convergence point of the linear regression lines rather than from the intercepts on the axis of total resistance,[52] see inset of Figure 5.

In staggered OFETs, the gate-voltage dependent R_c has been observed to mainly arise from two factors: bulk conductivity modulation and current crowding.[43] At small gate bias, the bulk semiconductor between contacts and channel would be highly resistive if the injected charges are limited, and the injection is confined in a small contact area close to the channel. Applying higher gate biases, charges accumulate in the channel but also spread far from the channel interface and thus increase the bulk conductivity at contacts. Meanwhile, charge injection extends to larger contact area, as injection current gets more and more crowded. In fact, the two factors can be much weakened in the case of Ohmic contacts because injection is so efficient that high gate bias is not obligatory to improve the bulk conductivity and to enlarge injection area. Thus, the very low and gate-voltage independent R_c in our n-doped PCBM devices signifies Ohmic contacts.

To more quantitatively explore the charge injection we calculated the charge concentration as well as the thickness of the depletion layer in semiconductor film at each doping level, based on the experimentally measured E_F (see Table 1). When the metal electrode is brought into contact

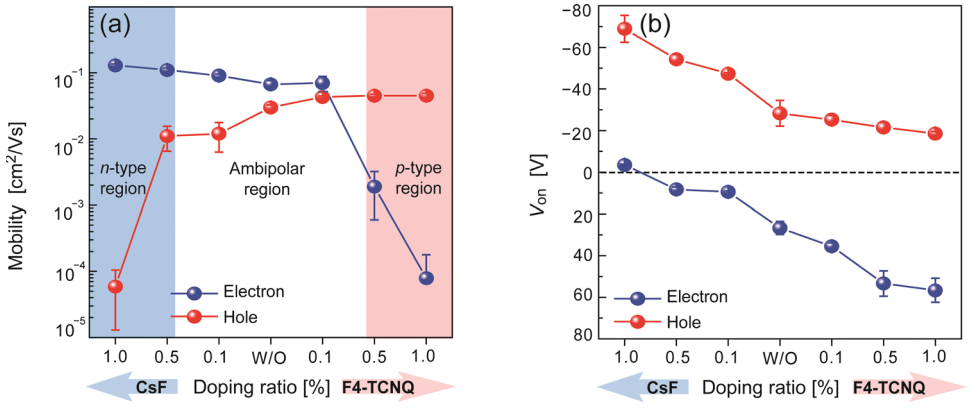

Figure 3. a) The evolution of electron and hole mobilities (μ_{FET}) in doped PCBM OFETs varying doping ratio and b) corresponding turn-on voltage (V_{on}).

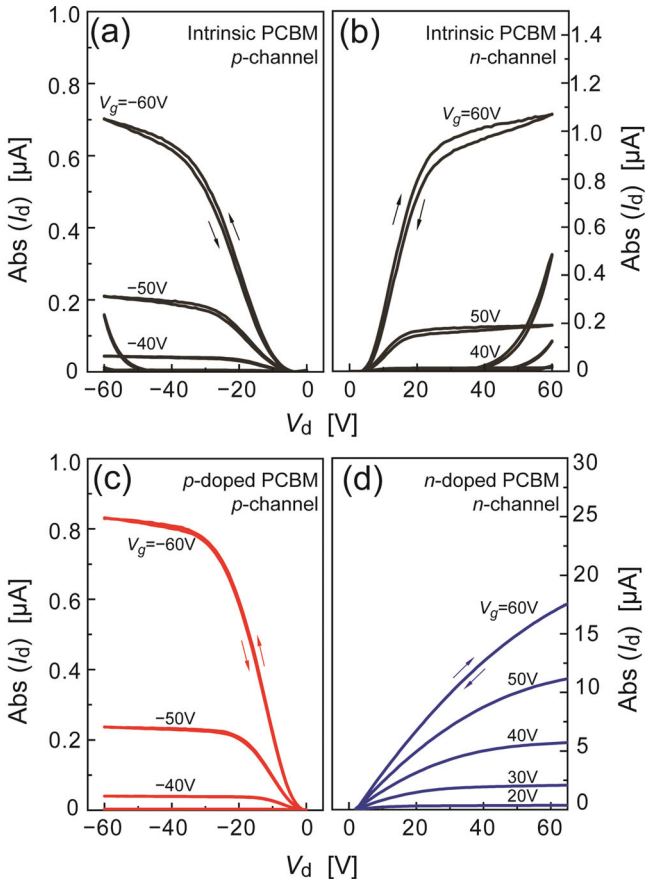

Figure 4. Output characteristics for a) p-channel and b) n-channel of undoped PCBM OFETs. c) p-channel of F4-TCNQ-doped PCBM OFETs. d) n-channel of CsF-doped PCBM OFETs.

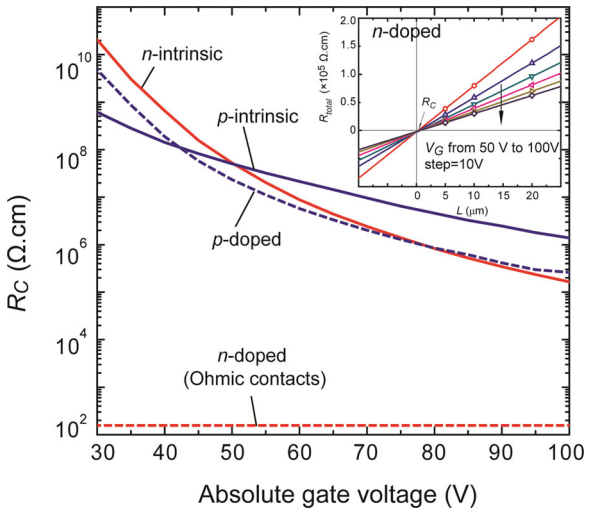

Figure 5. R_c of TG/BC PCBM OFETs varying the gate-voltage (red solid line: n-channel of intrinsic PCBM OFETs, red dashed line: n-channel of n-doped PCBM OFETs, blue solid line: p-channel of intrinsic PCBM OFETs, blue dashed line: p-channel of p-doped PCBM OFETs). Inset: R_c extracted by using M-TLM of n-doped (CsF) PCBM OFETs.

with the semiconductor, their respective E_F have to line up throughout the entire system at equilibrium through an interfacial exchange of charge which leads to the depletion of specific charge carriers in the semiconductor.[45] As schematically shown in **Figure 6**a, the depletion thickness is rather thick for the intrinsic PCBM OFETs (e.g., >1 μm) so that the charge carriers (both electrons and holes) have to be injected above large barriers, resulting in the high R_c and non-linearity in output curves for undoped devices. However, by introducing substantial n-type doping, the E_F shifts very close to the LUMO level. This implies high electron concentration at equilibrium, up to ~10^{19} cm^{-3}, a level similar to what can be achieved in the devices under study through electrostatic doping. The depletion thickness is significantly reduced to around 4 nm and efficient electron injection by direct tunneling becomes predominant (Figure 6b).[31,42,53] This is also very similar to the Ohmic contacts obtained in silicon MOSFETs by selectively heavy doping of contact areas. Once tunneling occurs, the electron injection barriers based on the framework of Schottky-Mott model will no longer matter. Note that n-doping does not affect the injection properties of holes and they are always thermally activated over the same energy barrier. Even though p-doping also shifts the E_F towards the HOMO level, the corresponding E_F is still located in the upper half of band gap since undoped PCBM exhibits as native n-type semiconductor. Furthermore, F4-TCNQ appears not to be able to provide enough acceptors to attain a good p-type semiconductor, probably due to high density of donor-like energy states around midgap which hinder a further shift of E_F towards the HOMO. As a consequence, E_F still stays close to midgap and the injection properties for holes are not significantly changed as compared with their initial conditions before doping. Therefore, doping has the twofold effect of improving the injection and the channel transport by filling highly localized intra-gap states, as discussed above and shown in Figure 6.

To further investigate the beneficial effects of chemical doping, the bias and ambient stabilities of doped PCBM OFETs were monitored by measuring the channel currents as a function of time. **Figure 7**a,b shows normalized I_d of pristine and CsF- and F4-TCNQ-doped PCBM OFETs under the constant bias condition at V_g = 60 V and V_d = 20 V (for n-channel) and at V_g = −60 V and V_d = −20 V (for p-channel) for 2000 s. The bias and ambient stability of both p- and n-channel devices are improved with doping, in particular the improvement is significant in the n-doped devices. The normalized I_d of n-channel CsF-doped devices decayed merely by ≈6% from its initial value, in sharp contrast to ≈57% decay of the undoped devices under the same bias stress. The bias-induced instability mainly originate from trap states of various sources, such as in active semiconductor and/or gate dielectric, and at their interfaces.[54,55] Because all devices studied here were fabricated with the same nominal conditions and configurations except for doping levels, it can be argued that the introduction of CsF dopant remarkably reduces the trapping of mobile charges in the semiconductor film, due to the filling of deep localized states as an effect of the E_F shift towards the LUMO.[31] In Figure 7b, the bias stability of F4-TCNQ-doped p-channel devices also display an improvement, though minor, with a ≈65% decay after 2000 s biasing in comparison with that of undoped PCBM device (≈80% decay). In the light of the previous explanation, the promotion of a much lower density of excess carriers upon

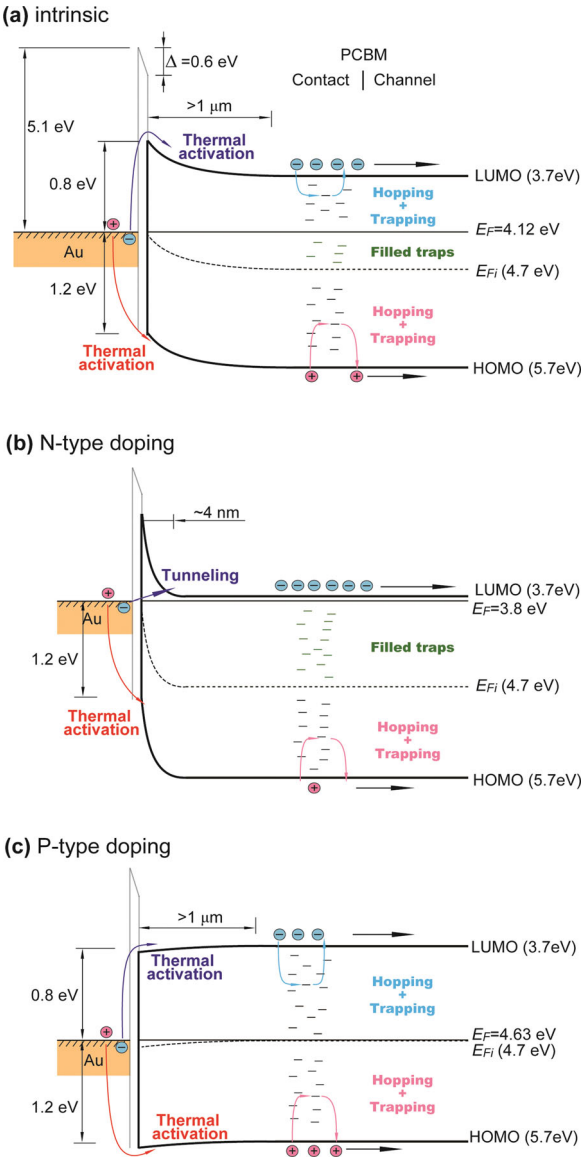

Figure 6. Schematic energy level alignment as derived from UPS data for PCBM and Au electrode junctions. a) Intrinsic PCBM. b) n-doped PCBM. c) p-doped PCBM.

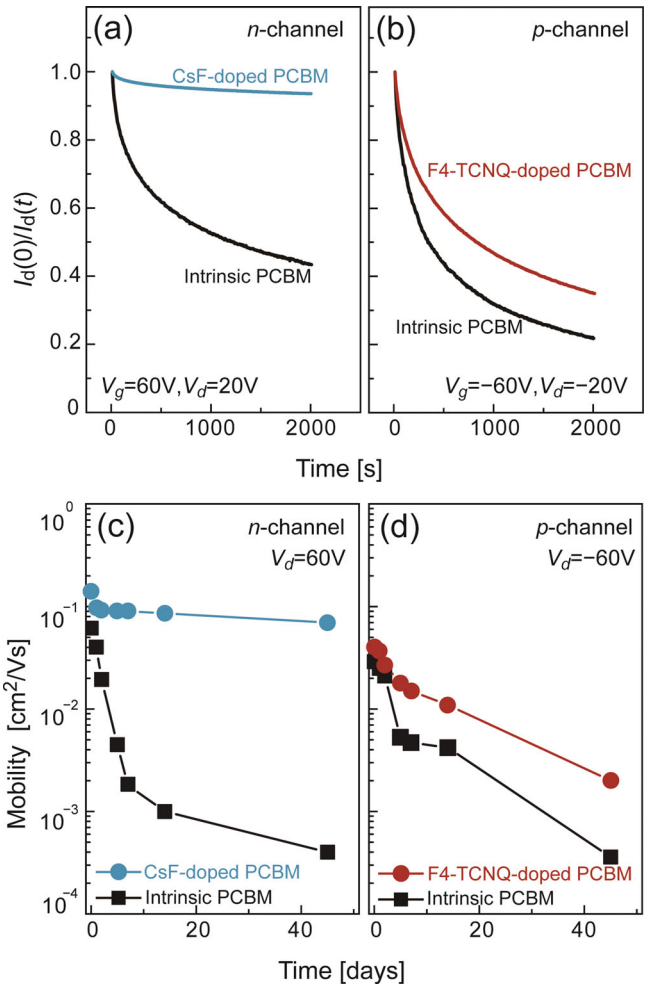

Figure 7. Study of bias and ambient stability of intrinsic and doped PCBM OFETs. a) Normalized current under the constant bias stress for intrinsic and CsF-doped PCBM OFETs at $V_g = 60$ V, $V_d = 20$ V for n-channel regime, and b) for intrinsic and F4-TCNQ-doped PCBM OFETs at $V_g = -60$ V, $V_d = -20$ V for p-channel regime. c) The change of field-effect mobility in air as function of time for intrinsic and CsF-doped PCBM OFETs at $V_d = 60$ V for n-channel regime and d) intrinsic and F4-TCNQ-doped PCBM OFETs at $V_d = -60$ V for p-channel regime.

F4-TCNQ doping (see Figure 6c, E_F still stays close to midgap), cannot prevent significant trapping of mobile charges even in doped p-channel PCBM OFETs.

In addition, we found a similar tendency in ambient stability test. There have been a few reports on improvement of the air-stability in OFETs by doping.[38,39] As it can be seen in Figure 7c,d, CsF-doped devices show better stability in ambient air than undoped ones, even though the CsF itself shows poor air stability due to its hygroscopic nature.[56] After 45 days of continuous air exposure, the $\mu_{FET,e}$ of CsF-doped PCBM OFETs decreased only to 0.070 $cm^2\ V^{-1}\ s^{-1}$ from the initial value of 0.14, whereas that of undoped devices was severely degraded from 0.062 to 0.0004 $cm^2\ V^{-1}\ s^{-1}$ under the same conditions. In parallel with gate-bias stress tests, F4-TCNQ doped devices showed only a limited ambient stability improvement: $\mu_{FET,h}$ dropped from 0.040 to 0.002 $cm^2\ V^{-1}\ s^{-1}$, however, a markedly lower decrease than for the case of undoped devices, going from 0.029 to 0.00036 $cm^2\ V^{-1}\ s^{-1}$. These results suggest that bias and ambient stability of ambipolar OFETs can be highly improved by molecular doping via filling of trap states by chemically induced excess carriers.

We further exploited the possibility to unipolarize and optimize complementary devices based on the same PCBM semiconductor by developing a selective molecular doping process by means of inkjet printing. The fabrication process flow is schematically represented in **Figure 8**a. The most fascinating feature of this approach is that we can induce balanced n- and p-channel characteristics, as the one required for complementary inverters, by selectively controlling the doping level through the local jetting of the desired dopant droplets on top of a predeposited semiconducting layer, which can be simply coated with another technique on the all circuit area. The doping level

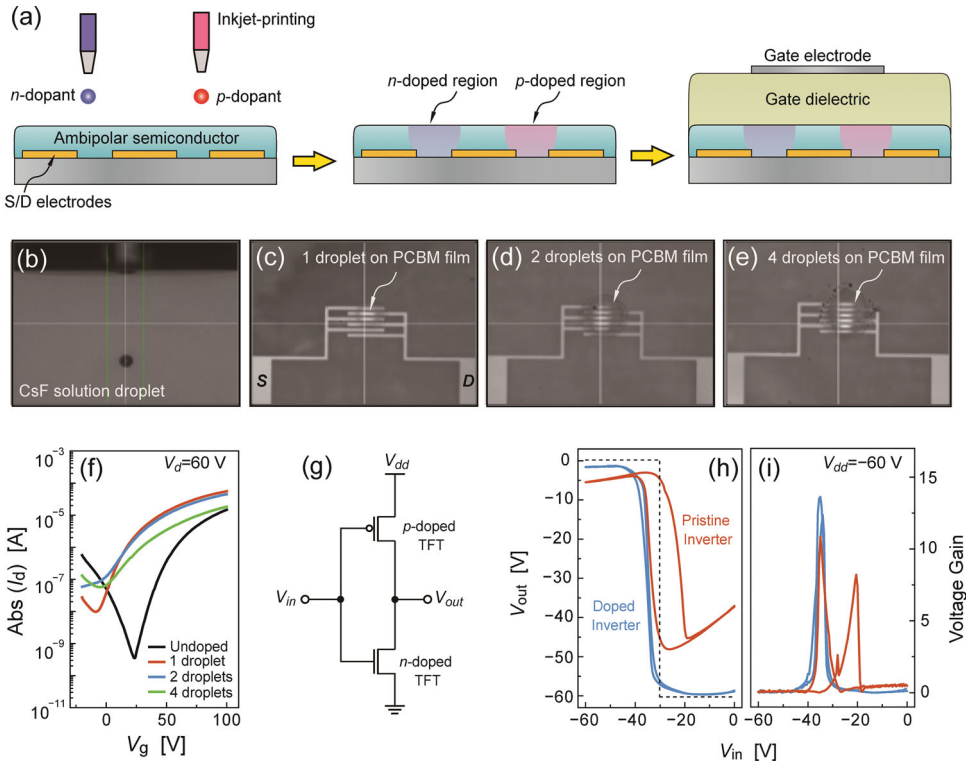

Figure 8. a) Schematic diagram of fabrication process flow and cross-sectional view of the complementary ambipolar inverter with a selective molecular doping method by means of inkjet printing. CCD camera images: b) of the CsF solution droplet by inkjet printing (average diameter of droplet ≈30 μm), c) of the CsF inkjet-printed onto pre-deposited PCBM thin film (1 droplet), d) 2 droplets, and e) 4 droplets. f) Transfer Characteristics of CsF inkjet-printed PCBM OFETs by varying the jetting number. g) Circuit configuration of the complementary-like inverter based on doped TFTs. h) Voltage transfer characteristics (VTCs) and i) corresponding voltage gains of inverters based on two identical PCBM FETs (orange solid line), n- and p-doped PCBM FETs by inkjet-printed doping method (blue solid line), and ideal inverter curves (black dashed line) at V_{dd} = –60 V.

could be tuned by controlling the concentration of dopant solution, number of jetted dopant droplets, and volumes of jetted dopants. In our experiment, CsF ink (≈1 mg mL^{-1} in CB) was inkjet-patterned onto the PCBM-coated transistor regions (average diameter of droplet was ≈30 μm as shown Figure 8b). The detailed description of fabrication process is included in Experimental Section. Figure 8c–e shows CCD camera images of CsF inkjet-printed PCBM surface by varying the jetting numbers and Figure 8f shows transfer characteristics of corresponding PCBM OFETs. As shown in Figure 8c, PCBM transistor regions were partially dissolved and sequentially solidificated by one CsF droplet, where CsF and PCBM could be blended, possibly enabling the n-doping of semiconductor. PCBM OFETs with one CsF droplet deposited by inkjet printing were successfully converted from initially ambipolar devices to n-doped, unbalanced devices with improved n-channel saturation current and reduced p-channel current. However, two CsF droplets could not improve the n-channel current and resulted in a slight increase of off-current level, similarly to heavily n-doped devices based on a blend with 2.0 wt% CsF. The printing of four CsF droplets even deteriorated the device performance, likely owing to partial etching of the PCBM film in the channel area or to a reduction in crystallinity following the repeated deposition of CsF ink droplets in the same position. Diffusion of dopants along the molecular stacks could limit stability and reliability of various organic devices.[31] In inkjet-printed doping system, especially, it may be possible to occur in undesirable diffusion of dopants from the doped region to the undoped region, because of the locally introduced doping. To verify the stability of locally doped OFETs via inkjet printing, we also monitored bias stability of inkjet-printed CsF-doped PCBM OFETs for a long time. Interestingly, inkjet-doped OFETs showed high bias stability similar to the blend-doped devices (see Figure S4 in Supporting Information). The normalized I_d of n-channel inkjet-printed CsF-doped devices decayed by ≈7% from its initial value in contrast to ≈57% decay of the undoped devices under the same bias stress for 2000 s and after even further bias stress for 4000 s, decayed only by ≈9%.

In order to produce p-doped PCBM OFETs, an F4-TCNQ ink also was inkjet-printed following the same procedure. A single droplet of F4-TCNQ ink is effective in turning the device characteristics from ambipolar into p-doped, unbalanced characteristics with suppressed electron conduction (See Figure S5 in Supporting Information). These results enabled the fabrication of complementary inverters with n-doped and p-doped PCBM OFETs by local inkjet printing of dopants. As a control device, complementary-like inverter integrating the pristine ambipolar PCBM layer exhibited non-ideal, *Z*-shaped voltage transfer characteristics (VTC), with large hysteresis, as shown in Figure 8h. The abnormal *Z*-shaped VTC and the large hysteresis are attributed to the presence of parasitic p-channel (n-channel) leakage current and unstable V_{th} for the n- and p-channel operation

modes of PCBM ambipolar FETs.[16] As a consequence, a large loss of output voltage (V_{out}) (≈23 V at V_{in} = 0 V and ≈6 V at high V_{in} = −60 V) and poor noise margins (27% of half of supply bias $^1/_2$ V_{dd} at V_{dd} = −60 V) were observed since neither of the two transistors in the inverter can be completely turned OFF as a consequence of the presence of an accumulated channel of one of the two carriers under all biasing conditions (See Figure S6b in Supporting Information).[23] Inverters based on n- and p-doped PCBM OFETs, on the other hand, exhibited a high gain and ideal VTC characteristics with a negligible hysteresis. V_{out} loss was also markedly decreased to ≈1 V at V_{in} = 0 V and ≈1.5 V at high V_{in} of −60 V, which resulted in noise margins as high as 67% of $^1/_2$ V_{dd} (See Figure S6a in Supporting Information). Through doping with CsF and F4-TCNQ, the operating modes of organic transistors based on an ambipolar π-conjugated material can be systematically controlled, thereby enabling the demonstration of truly complementary organic electronic circuitry based on a single semiconductor. To confirm the reproducibility of the performance of inverters by inkjet-printed doping method, we measured different 8 inverters fabricated by continuous inkjet printing process. Figure S7 in Supporting Information shows VTCs and voltage gain of inverters based on n- and p-doped OFETs by inkjet-printed doping methods. The VTC curves of all inverters exhibited very similar and the corresponding voltage gains are within a range of 13–20, which means that inkjet-printed doping methods are very reproducible and compatible with the consecutive printing process for large area electronics.

3. Conclusion

We have reported on controlled and selective optimization and unipolarization of staggered OFETs based on a single ambipolar semiconductor, either for p-channel or n-channel operation regimes, by molecular doping method. μ_{FET} and V_{on} both for electrons and holes in OFETs based on the ambipolar PCBM were precisely modulated by incorporating, either by blending or by inkjet printing on a pre-coated semiconductor, a small amount of dopants: CsF for n-channel OFETs and F4-TCNQ for p-channel OFETs. This effect is the result of the increase of thermally promoted excess carrier concentration induced by doping, shifting the E_F toward the respective transport energy levels and thus populating deep intra-gap levels that would otherwise act as traps for electrostatically induced carriers in the transistor. In particular, CsF-doped OFETs showed also Ohmic contact behavior, as a result of a strongly reduced depletion thickness between Au and doped PCBM interface. Interestingly, doped OFETs also showed greater stability under gate-bias stress and ambient conditions as compared to pristine ones, likely owing to the compensation of trap states. Finally, we took full advantage of this approach to realize complementary inverters by selective n- and p-doping via inkjet printing on a previously deposited pristine PCBM layer. The inverters based on locally doped complementary devices showed a high voltage gain of ≈14 and an excellent noise margin of 67% of the maximum value, $^1/_2$ V_{dd}. The molecular doping technique described here proved to be a promising methodology to obtain highly stable OFETs and complementary integrated circuits under bias-stress in ambient atmosphere. These results show that inkjet-printed molecular doping methods are a simple yet effective methodology for the development of high performance printed opto/electronic devices.

4. Experimental Section

Device Fabrication: Source and drain (S/D) electrodes of Au/Ni (12 nm/3 nm) were patterned on glass substrates (Corning Eagle 2000) by conventional lift-off photolithography technique. After cleaned in an ultrasonic bath with sequentially de-ionized water, acetone and isopropanol, the S/D patterned substrates were treated with oxygen plasma. The ambipolar semiconductor of PCBM was purchased from Nano-C Inc. and used as received. PCBM was dissolved in chlorobenzene (CB) to obtain 10mg/mL solution. CsF (Sigma Aldrich) and F4-TCNQ (Sigma Aldrich) were used as n- and p-dopant, respectively, and individually dissolved in 2-ethoxyethanol or CB. In order to make doped PCBM solution, blending of PCBM and dopant solutions (0.1, 0.5, 1.0, and 2.0 wt%) was prepared by mixing the two separated solutions, and then subsequently shaking was performed to obtain a homogenously mixed blend system at 80 °C for overnight. The undoped and doped PCBM solutions were spin-coated onto patterned glass substrate as active layers and then annealed at 100 °C for 20 min. For the polymer gate dielectric, CYTOP was spin-coated (≈480 nm), and baked at 80 °C for 1h to remove residual solvent. TG/BC OFETs were completed by forming gate electrodes on the channel region by evaporation of thin Al film (50 nm) using metal shadow masks. In order to fabricate the inverters based on doped, unipolar FETs, CsF- and F4-TCNQ-solution were selectively inkjet-printed on top of the pre-coated PCBM thin film. The CsF and F4-TCNQ were dissolved in CB or 2-ethoxyethanol to obtain 1mg mL^{-1} of solution and inkjet-printed onto transistor region in air using single nozzle (piezoelectric type, Microfab Inc.) inkjet printer (Unijet, Korea) with an orifice diameter of 50 μm. The jetting number of dopant solution were controlled for appropriate doping level and minimizing the adverse effect on underlying PCBM thin film by jetted solution. After ink-jetting the dopant onto semiconductors, PCBM thin films were annealed at 100 °C for 20 min. As a control device, inverters based on undoped PCBM were fabricated by spin-coating of the semiconductor layer. The thermal annealing, gate dielectric coating, and deposition of Al gate electrode were performed in the same manner for fabrication of individual OFETs.

Thin Film and Device Characterization: The electrical characteristics of OFETs and Inverters were measured using a Keithley 4200-SCS in a nitrogen-filled glove box. The μ_{FET} and V_{Th} were calculated in the saturation regime using a gradual channel approximation equation. The UPS measurements were carried out using AXIS-NOVA (Kratos, Inc.) with a base pressure of 4.2×10^{-9} Torr. The surface morphology of PCBM thin fims was investigated via tapping mode AFM (Nanoscope III, Veeco Intrument, Inc.) at the Korea Basic Science Institute (KBSI).

Carrier Concentration and Depletion Width Calculation: The numerical calculation was based on the conventional semiconductor device physics. The electron concentrations after n-type doping is $N_d = n_i \exp[(E_f - E_{fi})/kT]$ and the corresponding hole concentration is $N_a = n_i^2/N_d$, where $n_i = (N_C N_V)^{0.5} \exp[-(E_g/2kT)]$ is the intrinsic carrier concentration at thermal equilibrium with N_C (= 10^{21} cm^{-3}) and N_V (= 10^{21} cm^{-3}) being the density of states in conduction band and valence band, respectively, and E_g (= 2 eV) being the band gap of PCBM, k (= 8.6×10^{-5} eV K^{-1}) being the Boltzmann constant and T (= 300 K) being the absolute temperature. In the above, E_f and E_{fi} represent the Fermi level and the intrinsic Fermi level, respectively. The former was experimentally determined and the latter is calculated from the PCBM's LUMO (3.7 eV below vacuum level) and HOMO (5.7 eV below vacuum level) taken from UPS results and the literature. For this n-type doping the depletion width in the PCBM for Au/PCBM Schottky-like contact is $W_d = [2\varepsilon_{sc}(\Phi_m - E_f)/qN_d]^{0.5}$, where ε_{sc} (= 3.9) is the dielectric constant of PCBM relative to vacuum, Φ_m (= 4.5 eV) is the work function of contact electrode of

Au with taking account of an interface dipole of 0.6 eV between Au and PCBM, and q (= 1.6×10^{-19} C) is the electron charge. For p-type doping, the calculation was performed similarly.

Supporting Information

Supporting Information is available from the Wiley Online Library or from the author.

Acknowledgements

This research was financially supported by the National Research Foundation of Korea (NRF) grant funded by the Korean Government (MSIP) (NRF-2014R1A2A2A01007159), by the Center for Advanced Soft-Electronics (2013M3A6A5073183) funded by the Ministry of Science, ICT & Future Planning, the National Research Foundation of Korea (NRF) grant funded by the Korea government (MSIP) (No. 2013-059210) and the Dongguk University Research Fund of 2014.

Received: March 16, 2014
Revised: April 23, 2014
Published online: August 15, 2014

[1] J. Zaumseil, H. Sirringhaus, *Chem. Rev.* **2007**, *107*, 1296.
[2] T. D. Anthopoulos, D. M. de Leeuw, E. Cantatore, S. Setayesh, E. J. Meijer, C. Tanase, J. C. Hummelen , P. W. M. Blom, *Appl. Phys. Lett.* **2004**, *85*, 4205.
[3] J. Cornil, J.-L. Bre´das, J. Zaumseil, H. Sirringhaus, *Adv. Mater.* **2007**, *19*, 1791.
[4] M.-H. Yoon, C. Kim, A. Facchetti, T. J. Marks, *J. Am. Chem. Soc.* **2006**, *128*, 12851.
[5] G. Eda, G. Fanchini, M. Chhowalla, *Nat. Nanotechnol.* **2008**, *3*, 270.
[6] M. C. Lemme, T. J. Echtermeyer, M. Baus, H. Kurz, *IEEE Electron Device Lett.* **2007**, *28*, 282.
[7] W. K. Koh, S. R. Saudari, A. T. Fafarman, C. R. Kagan, C. B. Murray, *Nano Lett.* **2011**, *11*, 4764.
[8] R. Martel, V. Derycke, C. Lavoie, J. Appenzeller, K. K. Chan, J. Tersoff, P. Avouris, *Phys. Rev. Lett.* **2001**, *87*, 256805.
[9] P. Avouris, M. Freitang, V. Perebeinos, *Nat. Photonics* **2008**, *2*, 341.
[10] S. Z. Bisri, C. Piliego, J. Gao, M. A. Loi, *Adv. Mater.* **2014**, *26*, 1176.
[11] H. Chang, Z. Sun, Q. Yuan, F. Ding, X. Tao, F. Yan, Z. Zheng, *Adv. Mater.* **2010**, *22*, 4872.
[12] H. Chang, Z. Sun, M. Saito, Q. Yuan, H. Zhang, J. Li, Z. Wang, T. Fujita, F. Ding, Z. Zheng, F. Yan, H. Wu, M. Chen, Y. Ikuhara, *ACS Nano* **2013**, *7*, 6310.
[13] L.-L. Chua, J. Zaumseil, J.-F. Chang, E. C. -W. Ou, P. K.-H. Ho, H. Sirringhaus, R. H. Friend, *Nature* **2005**, *434*, 194.
[14] T. B. Singh, F. Meghdadi, S. Gunes, N. Marjanovic, G. Horowitz, P. Lang, S. Bauer, N. S. Sariciftci, *Adv. Mater.* **2005**, *17*, 2315.
[15] T. Yasuda, K. Goto, K. Fujita, T. Tsutsui, *Appl. Phys. Lett.* **2004**, *85*, 2098.
[16] K.-J. Baeg, J. Kim, D. Khim, M. Caironi, D.-Y. Kim, I.-K. You, J. R. Quinn, A. Facchetti, Y.-Y. Noh, *ACS Appl. Mater. Interfaces* **2011**, *3*, 3205.
[17] X. Cheng, Y.-Y. Noh, J. Wang, M. Tello, J. Frisch, R. P. Blum, A. Vollmer, J. P. Rabe, N. Koch, H. Sirringhaus, *Adv. Funct. Mater.* **2009**, *19*, 2407.
[18] K.-J. Baeg, D. Khim, S.-W. Jung, M. Kang, I.-K. You, D.-Y. Kim, A. Facchetti, Y.-Y. Noh, *Adv. Mater.* **2012**, *24*, 5433.
[19] D. Khim, K.-J. Baeg, J. Kim, J.-S. Yeo, M. Kang, P. S. K. Amegadzea, M.-G. Kim, J. Cho, J.-H. Lee, D.-Y. Kim, Y.-Y. Noh, *J. Mater. Chem.* **2012**, *22*, 16979.
[20] J. Zaumseil, R. H. Friend, H. Sirringhaus, *Nat. Mater.* **2006**, *5*, 69.
[21] L. Burgi, M. Turbiez, R. Pfeiffer, F. Bienewald, H.-J. Kirner, C. Winnewisser, *Adv. Mater.* **2008**, *20*, 2217.
[22] E. J. Meijer, D. M. de Leeuw, S. Setayesh, E. Van Veenendaal, B. H. Huisman, P. W. M. Blom, J. C. Hummelen, U. Scherf, T. M. Klapwijk, *Nat. Mater.* **2003**, *2*, 678.
[23] K.-J. Baeg, M. Caironi, Y.-Y. Noh, *Adv. Mater.* **2013**, *25*, 4210.
[24] T. D. Anthopoulos, S. Setayesh, E. Smits, M. Colle, E. Cantatore, B. de Boer, P. W. M. Blom, D. M. de Leeuw, *Adv. Mater.* **2006**, *18*, 1900.
[25] D. Khim, H. Han, K.-J. Baeg, J. Kim, S.-W. Kwak, D.-Y. Kim, Y.-Y. Noh, *Adv. Mater.* **2013**, *25*, 4302.
[26] A. J. Kronemeijer, E. Gili, M. Shahid, J. Rivnay, A. Salleo, M. Heeney, H. Sirringhaus, *Adv. Mater.* **2012**, *24*, 1558.
[27] D. Khim, K.-J. Baeg, M. Kang, S.-H. Lee, N.-K. Kim, J. Kim, G.-W. Lee, C. Liu, D.-Y. Kim, Y.-Y. Noh, *ACS Appl. Mater. Interfaces* **2013**, *5*, 12579.
[28] C. B. Nielsen, M. Turbiez, I. McCulloch, *Adv. Mater.* **2013**, *25*, 1859.
[29] B. Lüssem, M. L. Tietze, H. Kleemann, C. Hoßbach, J. W. Bartha, A. Zakhidov, K. Leo, *Nat. Commun.* **2013**, *4*, 2775.
[30] K. Walzer, B. Maennig, M. Pfeiffer, K. Leo, *Chem. Rev.* **2007**, *107*, 1233.
[31] B. Lüssem, M. Riede, K. Leo, *Phys. Status Solidi A* **2013**, *210*, 9.
[32] J. Blochwitz, M. Pfeiffer, T. Fritz, K. Leo, *Appl. Phys. Lett.* **1998**, *73*, 729.
[33] S. Reineke, F. Lidner, G. Schwartz, N. Seidler, K. Walzer, B. Lüssem, K. Leo, *Nature* **2009**, *459*, 234.
[34] Y. Abe, T. Hasegawa, Y. Takahashi, T. Yamada, Y. Tokura, *Appl. Phys. Lett.* **2005**, *87*, 153506.
[35] E. Lim, B.-J. Jung, M. Chikamatsu, R. Azumi, Y. Yoshida, K. Yase, L.-M. Do, H.-K. Shim, *J. Mater. Chem.* **2007**, *17*, 1416.
[36] L. Ma, W. H. Lee, Y. D. Park, J. S. Kim, H. S. Lee, K. Cho, *Appl. Phys. Lett.* **2008**, *92*, 063310.
[37] E. J. Meijer, C. Detcheverry, P. J. Baesjou, E. van Veenendaal, D. M. de Leeuw, T. M. Klapwijk, *J. Appl. Phys.* **2003**, *93*, 4831.
[38] J. H. Oh, P. Wei, Z. Bao, *Appl. Phys. Lett.* **2010**, *97*, 243305.
[39] P. Wei, J. H. Oh, G. Dong, Z. Bao, *J. Am. Chem. Soc.* **2010**, *132*, 8852.
[40] F. Ante, D. Kälblein, U. Zschieschang, T. Canzler, A. Werner, K. Takimiya, M. Ikeda, T. Sekitani, T. Someya, H. Klauk, *Small* **2011**, *7*, 1186.
[41] Y. Cai, H. X. Wei, J. Li, Q. Y. Bao, X. Zhao, S. T. Lee, Y. Q. Li, J. X. Tang, *Appl. Phys. Lett.* **2011**, *98*, 113304.
[42] S. Olthof, W. Tress, R. Meerheim, B. Lüssem, K. Leo, *J. Appl. Phys.* **2009**, *106*, 103711.
[43] T. J. Richards, H. Sirringhaus, *J. Appl. Phys.* **2007**, *102*, 094510.
[44] J. Veres, S. D. Ogier, G. Lloyd, D. de Leeuw, *Chem. Mater.* **2004**, *16*, 4543.
[45] S. Braun, W. R. Salaneck, M. Fahlman, *Adv. Mater.* **2009**, *21*, 1450.
[46] T. D. Anthopoulos, C. Tanase, S. Setayesh, E. J. Meijer, J. C. Hummelen, P. W. M. Blom, D. M. de Leeuw, *Adv. Mater.* **2004**, *16*, 2174.
[47] C. Waldauf, P. Schilinsky, M. Perisutti, J. Hauch, C. J. Brabec, *Adv. Mater.* **2003**, *15*, 2084.
[48] N. Tessler, Y. Preezant, N. Noam Rappaport, Y. Roichman, *Adv. Mater.* **2009**, *21*, 2741.
[49] G. Horowitz, R. Hajlaoui, P. Delannoy, *J. Phys. III* **1995**, *5*, 355.
[50] H. Sirringhaus, *Adv. Mater.* **2005**, *17*, 2411.
[51] Y. Xu, R. Gwoziecki, I. Chartier, R. Coppard, F. Balestra, G. Ghibaudo, *Appl. Phys. Lett.* **2010**, *97*, 063302.
[52] C. Liu, Y. Xu, G. Ghibaudo, X. Lu, T. Minari, Y.-Y. Noh, *Appl. Phys. Lett.* **2014**, *104*, 013301.
[53] J. Blochwitz, T. Fritz, M. Pfeiffer, K. Leo, D. M. Alloway, P. A. Lee, N. R. Armstrong, *Org. Electron.* **2001**, *2*, 97.
[54] A. Sharma, S. G. J. Mathijssen, E. C. P. Smits, M. Kemerink, D. M. de Leeuw, P. A. Bobbert, *Phys. Rev. B* **2010**, *82*, 075322.
[55] H. Sirringhaus, *Adv. Mater.* **2009**, *21*, 3859.
[56] V. Polshettiwar, M. P. Kaushik, *Cat. Comm.* **2004**, *5*, 515.